APL MATERIALS 5, 036103 (2017)

Reducing adhesion energy of micro-relay electrodes by ion beam synthesized oxide nanolayers

Bivas Saha,[1,2] Alexis Peschot,[3] Benjamin Osoba,[3] Changhyun Ko,[1] Leonard Rubin,[4] Tsu-Jae King Liu,[3] and Junqiao Wu[1,2,a]
[1]*Department of Materials Science and Engineering, University of California, Berkeley, California 94720, USA*
[2]*Materials Sciences Division and Molecular Foundry, Lawrence Berkeley National Laboratory, Berkeley, California 94720, USA*
[3]*Department of Electrical Engineering and Computer Sciences, University of California, Berkeley, California 94720, USA*
[4]*Axcelis Technologies, Beverly, Massachusetts 01915, USA*

(Received 2 December 2016; accepted 28 February 2017; published online 9 March 2017)

Reduction in the adhesion energy of contacting metal electrode surfaces in nano-electro-mechanical switches is crucial for operation with low hysteresis voltage. We demonstrate that by forming thin layers of metal-oxides on metals such as Ru and W, the adhesion energy can be reduced by up to a factor of ten. We employ a low-energy ion-beam synthesis technique and subsequent thermal annealing to form very thin layers (~2 nm) of metal-oxides (such as RuO_2 and WO_x) on Ru and W metal surfaces and quantify the adhesion energy using an atomic force microscope with microspherical tips. © *2017 Author(s). All article content, except where otherwise noted, is licensed under a Creative Commons Attribution (CC BY) license (http://creativecommons.org/licenses/by/4.0/).* [http://dx.doi.org/10.1063/1.4978436]

Nano-electro-mechanical (NEM) switches (relays) have attracted significant attention in recent years due to their potential to overcome the energy-efficiency limit of complementary metal-oxide semiconductor (CMOS) digital logic circuits and technology.[1–4] Since relays operate with zero off-state leakage current and abrupt switching characteristics, overcoming the limitation of 60 mV/decade room temperature subthreshold swing for CMOS transistors, they can be used to dramatically lower the energy consumption of digital electronic circuits.[3,4] Several theoretical analyses and experimental works have been performed to design and demonstrate relays driven by piezoelectric,[2] electrostatic,[5] or magnetic forces[6] and to achieve lower operating voltage.[7] As all relays operate on the basic principle of formation and breaking of mechanical contacts, contact adhesion energy plays an important role in determining the performance and energy efficiency of a relay.[8,9] Studies also have been performed to understand the effects of contact area scaling and the dynamics of contact opening/closing.[9–11] A general understanding gained from such analyses[7,11] is that the minimum energy needed to switch a relay is proportional to the contact adhesive force ($F_{ad.}$). Therefore, reduction of the adhesion energy (E_{Ad}) is necessary to improve the energy efficiency of a relay.

Adhesion is dependent on many parameters, including the contacting electrode material(s). Process limitations as well as device performance requirements impose additional constraints on the choice of the material(s). For high endurance and good performance, we have used hard metals with high electrical conductivity, such as W and Ru, as contacting electrode materials in logic relays.[7] With a motivation to reduce the adhesion energy per unit area without dramatically reducing the relay on-state conductance, we show herein that ultra-thin metal-oxides (such as RuO_2 and WO_x) on Ru and W metal surfaces can significantly decrease adhesion energy, by up to an order of magnitude.

The Ru and W thin films (approximately 30 nm in thickness) were deposited onto 100 nm of oxidized silicon wafer substrates at room temperature, using the reactive rf-sputtering technique

[a]Author to whom correspondence should be addressed. Electronic mail: wuj@berkeley.edu

 © Author(s) 2017

inside a high vacuum chamber (3×10^{-6} Torr). To promote adhesion, a thin (1.5 nm thick) layer of TiO_2 was deposited onto the SiO_2 surface by atomic layer deposition (ALD) prior to Ru deposition. No adhesive layer was used for W, since it adheres well to SiO_2. To form oxide on a metal surface, low-energy oxygen-ion implantation followed by thermal annealing at 450 °C for 30 min in forming gas (95% N_2 and 5% H_2) was employed. The ion implantations were performed with 7° tilt angle and acceleration energies of 3 keV for Ru and 3.5 keV for W samples, respectively. These energies were selected based on Stopping and Range of Ions in Matter (SRIM) simulations,[12] to achieve a projected implant range of ~2–3 nm. (See Fig. S1 in the supplementary material for SRIM-simulated range *vs.* energy, and an example of oxygen depth distribution in Ru. It should be noted that for such low acceleration energies, the longitudinal and lateral straggles are comparable in magnitude to the projected range.) Two values of O_2 implant dose were investigated for each metal: 4.5×10^{15} cm^{-2} and 7.3×10^{15} cm^{-2} for Ru; 4.2×10^{15} cm^{-2} and 7.0×10^{15} cm^{-2} for W. As an additional experimental split condition, the substrate temperature was either cooled or not cooled during implantation. Atomic force microscopy (AFM) was used to measure adhesive force between contacting materials (metal/metal-oxide and AFM tip) in the force spectroscopic mode.[13] The measured adhesive force and the RMS surface roughness were used to calculate the adhesion energy. Material properties of the oxides, such as their composition and thicknesses, were determined by X-ray photoelectron spectroscopy (XPS).

Microspherical SiO_2 tips (inset in Fig. 1(a)) with 2 μm tip diameter were used for the AFM measurements. The bare SiO_2 tips were later coated with Ru or W using the same recipe as used to deposit these metals onto oxidized silicon wafer substrates, for measurements of adhesive force between related materials (for example, Ru-Ru contact or RuO_2-Ru contact). The relatively large tip diameter provides for consistent measurements of contact adhesive force, in contrast to more conventional sharp AFM tips with smaller diameters (less than 10 nm) that are used for tapping-mode measurements of surface topology. Using a small-diameter tip, we observed significant variations in measured adhesive force from area to area, and even within the same area of the sample. (See Fig. S2 in the supplementary material for details.)

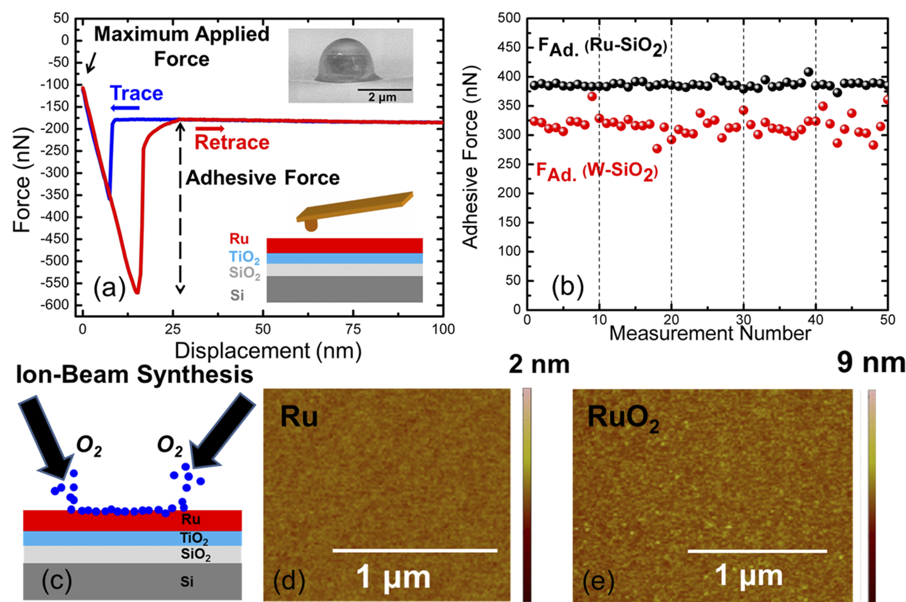

FIG. 1. (a) Representative force-*vs.*-displacement plot for AFM-based adhesion measurement, with the adhesive force and maximum applied force indicated. Upper inset shows a scanning electron microscopy image of the SiO_2 microspherical AFM tip with 2 μm diameter. Lower inset shows a schematic of the measured sample structure. (b) Measured adhesive force across 50 measurements, for Ru and W metal films contacted with a bare SiO_2 AFM tip. (c) Schematic illustration of the ion-beam synthesis process to form an ultra-thin layer of oxide on the metal surface. (d) AFM image of the Ru metal film surface. (e) AFM image of the oxidized Ru (RuO_x) film surface. The RMS roughness of the surfaces was measured using conventional tapping-mode AFM with a sharp tip of ~8 nm diameter.

A typical force-*vs*.-displacement plot obtained with a microspherical SiO_2 tip and Ru film is presented in Fig. 1(a), wherein the trace and retrace curves correspond to the approach and retraction of the tip to/from the Ru surface, respectively. For each of the adhesion measurements, the maximum applied force was 100 nN. The rationale for this is discussed below. The adhesive force was determined from the retrace curve as shown in Fig. 1(a). To check for reproducibility, 10 measurements were performed at each of 5 randomly chosen spots on each sample. The results for Ru(film)-SiO_2(tip) contact and W(film)-SiO_2(tip) contact are presented in Fig. 1(b). For Ru, the measurements are very consistent at 386 nN on average, with a standard deviation of 5 nN. For W, there is a greater variation, with a standard deviation of 16 nN for an average adhesive force of 316 nN. This is attributed to the larger RMS surface roughness of the W film (0.45 nm) as compared against the Ru film (0.21 nm), as deduced from AFM measurements (e.g., Fig. 1(d)), since larger surface roughness results in larger differences in the contact environment from measurement to measurement. Nevertheless, the variation in measured values of adhesive force is relatively small (less than 5%), for all of the samples studied in this work.

Adhesive force between materials has several origins including (1) van der Waals force, (2) chemical interaction forces due to bonding between the atoms of the materials, (3) electrostatic interactions, and (4) capillary force due to external contaminants such as water and polymers on the sample surfaces.[14] While the first three are intrinsic, the fourth can be mitigated with proper care. Hence the adhesion measurements were performed in a dry-N_2 environment. (Prior to measurement, the sample was *in situ* heated to 140 °C for several hours and then cooled to room temperature under dry-N_2 flow.) The capillary force was found to contribute less than 12% to the total adhesive force (see Fig. S3 in the supplementary material).

The adhesion energy per unit area, which is an absolute gauge of the adhesion property of a material, was calculated using the Derjaguin-Muller-Toporov (DMT) continuum mechanics model.[14,15] The effect of surface roughness was accounted for using the modified-Rumpf model[16,17] since it is best suited for solid materials with surface roughness values less than 2 nm.[17] In this model, the roughness is approximated as a single hemispherical asperity on a flat surface; the radius of the asperity depends only on the RMS roughness of the surface.[15,17] The equation combining the DMT and modified-Rumpf model is[13]

$$W_{Ad.} = \left(\frac{F_{Ad.}}{2\pi R_{tip}}\right) \frac{\left(1+\frac{R_{tip}}{1.48R_{atomic}}\right)^{-1} + \left(1+\frac{1.48R_{atomic}}{z_0}\right)^{-2}}{\left(1+\frac{R_{tip}}{1.48R_q}\right)^{-1} + \left(1+\frac{1.48R_q}{z_0}\right)^{-2}}, \tag{1}$$

where $W_{Ad.}$ is the adhesion energy per unit area, $F_{Ad.}$ is the adhesive force determined from AFM measurements, R_{tip} is the radius of the AFM tip, R_{atomic} and R_q are the RMS roughness values of the sample surface and the tip, respectively, and z_0 is the equilibrium separation distance between the tip and the sample when they are in contact. A value of 0.32 nm was used for z_0 for all contact cases in this work, which represents the c-axis lattice parameter[18] of RuO_2. For the bare SiO_2 tip, a roughness value of 0.3 nm was used. A sensitivity test of the SiO_2 RMS roughness was performed, which showed that the percentage adhesion energy reduction by oxidation of the metal is insensitive to the tip roughness, as expected. However, the adhesion energy values of the individual sample-tip contacts depend on the tip roughness value assumed. For the Ru- or W-coated tip, the roughness value of the metal thin film was used. The RMS roughness of the implanted and annealed RuO_2 sample was measured to be 0.55 nm, while the WO_x film has an RMS roughness of 1.51 nm.

Calculated values of adhesion energy per unit area for contacts between metal or metal-oxide thin films and AFM tips (bare SiO_2, or coated with Ru or W) are presented in Fig. 2. The adhesion energy between Ru and SiO_2 is 92 mJ/m^2, whereas the adhesion energy between W and SiO_2 is about 3× lower, at 30 mJ/m^2. Fig. 2 also shows that the adhesion energies are ~3× and ~5× smaller for RuO_2 and WO_x in contact with SiO_2 (27 mJ/m^2 for RuO_2-SiO_2 and 5 mJ/m^2 for WO_x-SiO_2). Clearly, oxide formation on metal surfaces reduces adhesion energy. The results for RuO_x samples formed with different implantation conditions are very similar (within the error ranges—see Fig. S4 in the supplementary material). This is not altogether surprising, since the samples were annealed together after O_2 implantation so that the chemical compositions of the oxides formed on the surfaces are

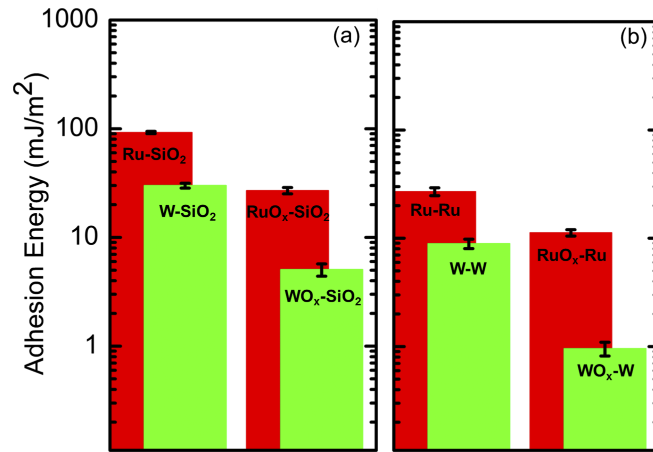

FIG. 2. Comparison of calculated values of adhesion energy per unit area for Ru, RuO_x (with x = 2 at the surface), W and WO_x contacted with (a) a bare SiO_2 AFM tip or (b) a metal-coated SiO_2 AFM tip.

expected to be very similar. Moreover, the RMS roughness values of the samples were found to be very similar. The adhesion energies for Ru-Ru and W-W contacts (i.e., deduced from measurements using an AFM tip coated with metal) are 27 mJ/m^2 and 9 mJ/m^2, respectively. Oxidation of the metal thin film surface reduces these to very low values of 11 mJ/m^2 and 1 mJ/m^2, respectively, similarly as for SiO_2 contacts. While the measurements and calculated results clearly show a decrease in adhesion energy of oxidized vs. pristine surfaces, one should not compare measurements made with different tips (e.g., SiO_2 tip versus Ru tip), as deposition of coating material on the tip will change the tip properties and alter the nature of tip-sample interaction, and hence influence the obtained adhesion values.

Reduction in adhesion energy due to oxide formation on a metal surface could be due to several factors. We believe that the reduction of chemical interaction forces plays an important role in the reduction mechanism. In addition, van der Waals forces and Casimir forces could also be reduced as a result of oxide formation and the resultant lower electrical conductivity of the surface. The adhesion energy per unit area of an interface between two materials A and B is given by the following equation:[19]

$$W_{Ad.} = \sigma_A + \sigma_B - \gamma_{A-B}, \tag{2}$$

where σ_A and σ_B are the surface energies of the materials A and B, respectively, and γ_{A-B} is the energy of the interface between materials A and B. Most metals have high surface energy and low interface energy due to the presence of dangling bonds on the surface. Electrostatic attraction between conduction electrons of the contacting metals makes metal-metal bonds easy to form across the interface.[20] A phenomenological expression for the interaction potential of two similar metallic surfaces is[21]

$$W(D) = 2\sigma\left[1 - \frac{D - D_0}{\lambda_M}\right] e^{\frac{-(D-D_0)}{\lambda_M}}, \tag{3}$$

where λ_M is a characteristic decay length of the metal material, D is the distance between the metal surfaces, and D_0 is the equilibrium distance. Under the equilibrium condition, the adhesion energy is $W(D) = 2\sigma$. As a result, metal contacts generally have large adhesion energies. In contrast, oxides (like most ceramics) usually have nearly saturated surface bonds so that they have low surface energies. Also, oxide-oxide bonds are more covalent in character and are more difficult to form than metallic bonds. Therefore, oxide contacts typically have lower adhesion energies compared to metal contacts. Given this general description, it is not surprising that the formation of oxides on metal surfaces was found in this work to considerably reduce adhesion energies.

To determine the stoichiometry and thicknesses of the ion-beam synthesized oxides on the metal surfaces, we performed detailed XPS analyses to compare the O and Ru depth profiles in

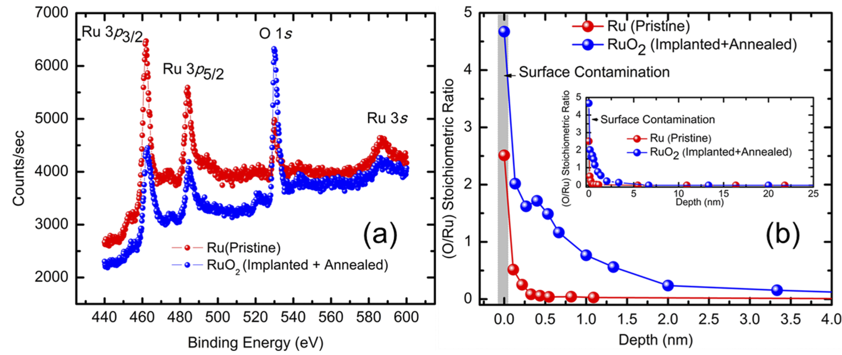

FIG. 3. (a) X-ray photoelectron spectra (XPS) of Ru and RuO_2 films (collected after gently removing the surface contamination layer) showing that the oxygen signal is significantly higher in the O_2-implanted and annealed sample *vs*. the pristine Ru sample, indicative of oxide formation in the former. (b) Comparison of O/Ru stoichiometric ratio depth profiles, showing that the surface of pristine Ru sample is not oxidized, in contrast to the O_2-implanted and annealed Ru sample.

a pristine Ru sample *vs*. an implanted and annealed sample. The results presented in Fig. 3 indicate that the pristine-Ru sample is very pure, with negligible native oxide on the surface; this is consistent with our previous experiments demonstrating that native RuO_x formation is a self-limiting process.[22] The results for the implanted and annealed sample indicate an oxide thickness of ~2 nm with a stoichiometry of RuO_2 at the surface, confirming the accuracy of the SRIM simulations.

Using the DMT model,[14,15] we have also estimated the effects of other parameters such as the contact radius (a), sample deformation (δ), and contact pressure (P) underneath the tip during measurement. The contact radius (a) for the AFM tip is given by the following expression:[15]

$$a = \sqrt[3]{\frac{R_{tip}}{E_{total}}(F + 2\pi R_{tip} W_{Ad.})}, \tag{4}$$

where E_{total} is the reduced elastic modulus, which is a combined elastic modulus that considers both the tip material and the sample material through the relation presented in Eq. (5), where v_s, E_s, v_t, and E_t are the Poisson's ratio and Young's moduli of the sample and tip, respectively,

$$\frac{1}{E_{total}} = \frac{3}{4}\left(\frac{1 - v_s^2}{E_s} + \frac{1 - v_t^2}{E_t}\right), \tag{5}$$

F is the applied force, and R_{tip} and $W_{Ad.}$ are the tip radius and the adhesion energy, respectively. We find that the contact radius of the AFM tip is approximately 25 nm, which gives a contact area of ~2000 nm^2 for 100 nN of applied force in a Ru-SiO_2 contact. Considering that the AFM tip radius is 1 μm, only a small portion (about 2.5%) of the tip is actually in contact with the sample surface when the applied force is 100 nN. However, our measurements show that 2000 nm^2 of contact area is sufficient for reproducible bond formation and breaking (from measurement to measurement), despite the aforementioned effect of surface roughening to increase variability. The deformation of the sample surface (δ) is given by the expression $\frac{a^2}{R_{tip}}$ and is approximately 0.63 nm for our measurements. Such a small deformation ensures that the materials are in the elastic regime, for accurate measurement of adhesion energy. The pressure underneath the tip is calculated to be ~350 bars during the measurements.

Adhesive force per unit area in a functional NEM relay has been extracted by Yaung *et al.*[8] and Lee *et al.*[23] using indirect methods such as electrical characterization and indirect AFM-based analysis wherein the force is applied on the movable electrode of the relay. While the results extracted from the electrical characterization showed an adhesive force of 0.02 nN/nm^2 between the W electrodes, the indirect AFM measurement showed a much lower adhesive force of 1.6×10^{-5} nN/nm^2. The direct AFM based experimental analysis performed here between W-W contacts shows that the adhesive force is about 0.17 nN/nm^2, which is an order of magnitude higher than the estimates by Yaung *et al.*[9] We believe that this difference is due to the assumptions used in estimating the

contact area: While Yaung *et al.*[8] have used the dimple (apparent) contact area for the calculation of force per unit area, here we use the DMT model to estimate the microscopic (real) contact area.

As the contact area increases with applied force, so should chemical interaction forces. To investigate this effect, we performed an experiment in which the applied force was increased from 100 nN to 1 μN. The results presented in Fig. 4 show that the RuO_2-SiO_2 adhesion energy increases with the applied force, by about 25%. Using the DMT model, we estimate that the corresponding increase in the contact area is about 44%. This suggests that the sample is plastically deformed for 1 μN of applied force. Therefore, an applied force of 100 nN was used to obtain all of the data presented in Fig. 2. (An applied force of 50 nN was found to be too small to yield reproducible measurements.) It should be noted that the contact force in NEM relays is a strong function of the relay operation mode and body-biasing condition and could range from a few micro-newtons to very small values (theoretically approaching zero when the body-bias voltage is close to the release voltage). Thus, the 100 nN applied force in our AFM measurements is within the range relevant for relay operation.

Logic relays should be stable and operate with high endurance, more than 10^{14} cycles,[24] in order to have a broad application. In the previous work,[25] we demonstrated that relays with Ru contacts can operate with sufficient on-state conductance for at least 10^8 cycles, under low vacuum conditions. Stability of contact adhesion is also critical for achieving highly reliable relay operation, since a large adhesive force can cause a relay to be stuck in the on state. We have therefore studied the evolution of adhesive force in a RuO_2-SiO_2 contact over the course of many operating cycles. Due to the low frequency (0.25 Hz) of the AFM measurement technique, we were able to monitor the contact for only 1000 cycles; nevertheless, the results provide insight into the stability of adhesion energy. The results presented in Fig. 4(b) show that the adhesive force remains stable over the 1000 operating cycles that is expected to result in efficient device performance. Adhesion cycling tests performed on bare-Ru/SiO_2 (shown in the supplementary material) indicate an increase in adhesive force by ~6% over the 1000 contact cycles, probably due to wearing of the tip, highlighting the benefit of oxides in terms of contact stability.

Having discussed the adhesion properties of the metals and metal-oxides, we now comment briefly on their electrical properties. Previous reports[22] indicate that RuO_2 (the only Ru oxide that is stable in atmospheric ambient) is electrically conductive, since it has a resistivity that is only a factor of seven higher than that of pure Ru, at room temperature. Considering that the ion-beam synthesized RuO_2 is only ~2 nm thick, and that a contact resistance of ~1 mΩ was measured between two RuO_2 disks with 1 cm diameter,[26] we would not expect it to dramatically increase the contact resistance. Also, oxide formation on Ru electrodes should help stabilize the stiction coefficient as a function of

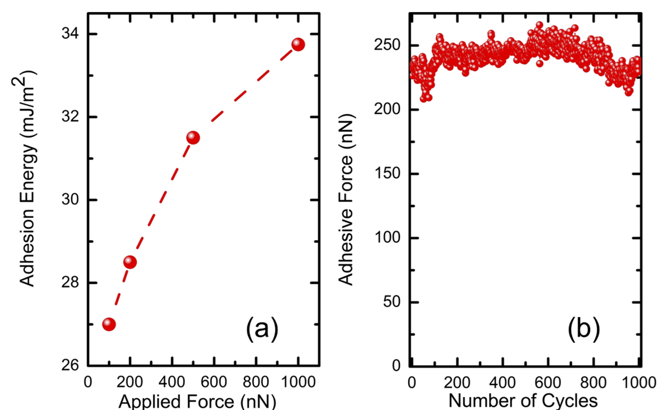

FIG. 4. (a) Adhesion energy for RuO_2-SiO_2 contact as a function of the applied force during the AFM measurement. (b) Evolution of contact adhesive force with the number of cycles, for a RuO_2 thin film contacted by a bare SiO_2 AFM tip with 0.25 Hertz frequency. Further experiments (not presented here) show that the characterization frequency of the AFM measurements does not affect the nature of the cycling test and the reliability of the measurements.

cycles under hot-switching conditions (see supplementary material). In contrast, WO_3 is known to be electrically insulating,[27] so the stoichiometry and thickness of the WO_x layer must be carefully controlled (by adjusting the O_2 ion implant dose and acceleration energy) to ensure a sufficiently high on-state electrical conductance.

In conclusion, we have demonstrated that low-energy ion beam synthesis and subsequent thermal annealing result in nanolayers of metal oxides (such as RuO_2 and WO_x) on Ru and W metal surfaces, and the adhesion energy of the metals can be reduced by up to a factor of ten through the formation of the oxide nanolayers. XPS analysis shows that the oxide nanolayers are ~ 2 nm thick and stoichiometric (for RuO_2 on the Ru metal surfaces), which is expected to result in low on-state resistance needed for relay operations. The adhesion energy is quantified using an AFM with microspherical tips. Reduction of the adhesion in NEM contact metals through oxide nanolayers is important not just for the relay switch applications, but also for several other types of MEMS devices including RF MEMS switches that rely on the contact between a conductive membrane and an insulating dielectric. Therefore, this technique can be used to improve the energy efficiency of a broad class of MEMS and NEMS devices.

See supplementary material for the details about SRIM simulation results, adhesion measurements with AFM tip of small diameter, quantification of capillary forces, effects of ion-implantation process parameters on adhesion, sensitivity test of SiO_2 probe tip roughness, contact cycling results of bare-Ru/SiO_2 adhesive force, effects of AFM contact frequency on measurements, possible effects of electrical current and triboelectric effect on contact adhesion, and possible packaging conditions of the NEM relays.

The work was supported by the Center for Energy Efficient Electronics Science (NSF Award No. 0939514). XPS experiments were performed at the Molecular Foundry of the Lawrence Berkeley National Laboratory, which was supported by the Office of Science, Office of Basic Energy Sciences of the U.S. Department of Energy under Contract No. DE-AC02–05CH11231. A. Peschot gratefully acknowledges post-doctoral fellowship support from the DGA. The authors declare no conflicts of interest.

[1] S. Han, V. Sirigiri, D. G. Saab, and M. Tabib, in *Proceedings of the International Conference on Computer-Aided Design (ICCAD)* (ACM, 2012), pp. 533–538.
[2] U. Zaghloul and G. Piazza, IEEE Electron Device Lett. **35**(6), 669–671 (2014).
[3] M. Spencer, F. Chen, C. C. Wang, R. Nathanael, H. Fariborzi, A. Gupta, H. Kam, V. Pott, J. Jeon, T. J. K. Liu, D. Markovic, E. Alon, and V. Stojanovic, IEEE J. Solid-State Circuits **46**(1), 308–320 (2011).
[4] F. Chen, H. Kam, D. Markovic, T. J. K. Liu, V. Stojanovic, and E. Alon, in *IEEE/ACM International Conference on Computer-Aided Design* (IEEE, San Jose, CA, 2008), p. 8.
[5] P. M. Osterberg and S. D. Senturia, J. Macroelectromech. Syst. **6**(2), 107–118 (1997).
[6] D. Niarchos, Sens. Actuators, A **109**(1–2), 166–173 (2003).
[7] C. Qian, A. Peschot, I. Chen, Y. Chen, N. Xu, and T. J. K. Liu, IEEE Electron Device Lett. **36**(8), 862 (2015).
[8] J. Yaung, L. Hutin, J. Jeon, and T.-J. K. Liu, J. Microelectromech. Syst. **23**(1), 198–203 (2014).
[9] B. Jensen, K. Huang, L. L. W. Chow, and K. Kurabayashi, J. Appl. Phys. **97**(10), 103535 (2005).
[10] A. Knoll, O. Zuger, and U. Duerig, New J. Phys. **14**, 123007 (2012).
[11] I-Ru. Chen, C. Qian, E. Yablonovitch, and T. J. K. Liu, IEEE Electron Device Lett. **36**(9), 963 (2015).
[12] J. F. Ziegler, J. P. Biersack, and M. D. Ziegler, *SRIM - The Stopping and Range of Ions in Matter* (Lulu Press, 2008).
[13] T. Jiang and Y. Zhu, Nanoscale **7**, 10760 (2015).
[14] H. Butt, B. Cappela, and M. Kappl, Surf. Sci. Rep. **59**, 1–152 (2005).
[15] T. D. B. Jacobs, K. E. Ryan, P. L. Keating, D. S. Grierson, J. A. Lefever, K. T. Turner, J. A. Harrison, and R. W. Carpick, Tribol. Lett. **50**, 81–93 (2013).
[16] O. Laitinen, K. Bauer, J. Niinimaki, and U. A. Peuker, Powder Technol. **246**, 545–552 (2013).
[17] Y. I. Robinovich, J. J. Adler, A. Ata, R. K. Singh, and B. M. Moudgil, J. Colloid Interface Sci. **232**, 10–16 (2000).
[18] X. Wang and R. G. Gordon, Cryst. Growth Des. **13**, 1316–1321 (2013).
[19] L. Lee, *Fundamentals of Adhesion* (Springer Science Press, 1991 and 2001).
[20] G. S. Rohrer, *Structure and Bonding in Crystalline Materials,* 1st ed. (Cambridge University Press, 2001).
[21] J. N. Israelachvili, *Intermolecular and Surface Forces* (Academic Press, 2011).
[22] I.-Ru. Chen, Y. Chen, L. Hutin, V. Pott, R. Nathanael, and T. J. K. Liu, in Transducer 2013, Barcelona, Spain, 16-20 June, 2013.
[23] D. Lee, V. Pott, H. Kam, R. Nathanael, and T. J. K. Liu, in *2010 IEEE 23rd International Conference on Micro Electro Mechanical Systems* (IEEE, 2010), pp. 232–235.
[24] Y. Chen, "Reliability studies of micro-relay for logic applications", Ph.D. dissertation (University of California, Berkeley, 2015).
[25] Y. Chen, R. Nathanael, J. Jeon, J. Yaung, L. Hutin, and T. J. K. Liu, J. Microelectromech. Syst. **21**(3), 511 (2012).
[26] R. G. Vadimsky, R. P. Frankenthal, and D. E. Thompson, J. Electrochem. Soc. **126**(11), 2017 (1979).
[27] K. Miyake, H. Kaneko, and Y. Teramoto, J. Appl. Phys. **53**(3), 1511 (1982).

Supplementary Material

Reducing Adhesion Energy of Micro-relay Electrodes by Ion Beam Synthesized Oxide Nanolayers

Bivas Saha[1,2], Alexis Peschot[3], Benjamin Osoba[3], Changhyun Ko[1,2], Leonard Rubin[4], Tsu-Jae King Liu[3] and Junqiao Wu[1,2,*]

1. Department of Materials Science and Engineering, University of California, Berkeley, CA 94720, United States
2. Materials Sciences Division and Molecular Foundry, Lawrence Berkeley National Laboratory, Berkeley, California 94720, United States
3. Department of Electrical Engineering and Computer Sciences, University of California, Berkeley, CA 94720, United States
4. Axcelis Technologies, Beverly, MA, 01915, United States

1. SRIM Simulations

The Stopping and Range of Ions in Matter (SRIM) simulation results on the oxygen implantation depth-*vs*.-implantation energy, as well as the oxygen distribution profiles are presented in Fig. S1. It is clear from both the figures that at ~3 keV of implantation energy, the expected depth of oxygen in Ru and W metals are around 2-3 nm as desired.

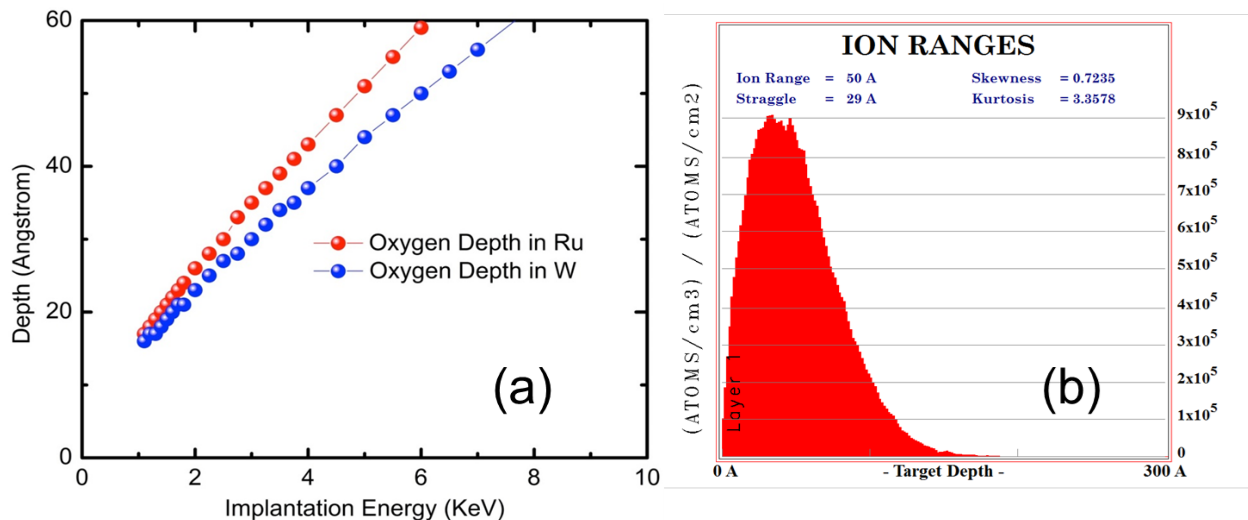

FIG. S1. (a) Oxygen implantation depth inside Ru and W films is presented as a function of the implantation energy calculated with SRIM simulations. It is clear from the figure that at ~3 keV implantation energy, the oxygen depth should be around 2-3 nm. (b) Oxygen distribution profile is presented as a function of the depth from the Ru sample surface.

2. Adhesion Measurement with AFM tip of Small Diameter

We chose to use microspherical SiO_2 AFM tips with a diameter of 2 μm for the adhesion measurements because conventional sharp AFM tips with a diameter of 8 nm (usually utilized for surface roughness measurements) do not yield consistent results, as can be seen from Fig. S2 which shows measured adhesive force values for a sharp SiO_2 AFM tip contacting a Ru sample (5 measurements in each of 5 different areas): the standard deviation is 16 nN, which is more than 20% of the average value of 76 nN. Such large variation is not surprising, since the contact area of the tip with the sample is only ~3 nm (calculated using the DMT model and equation 4) in the paper) so that the contact area and local environment can vary significantly from measurement to measurement, due to surface roughness, thermal drift and others.

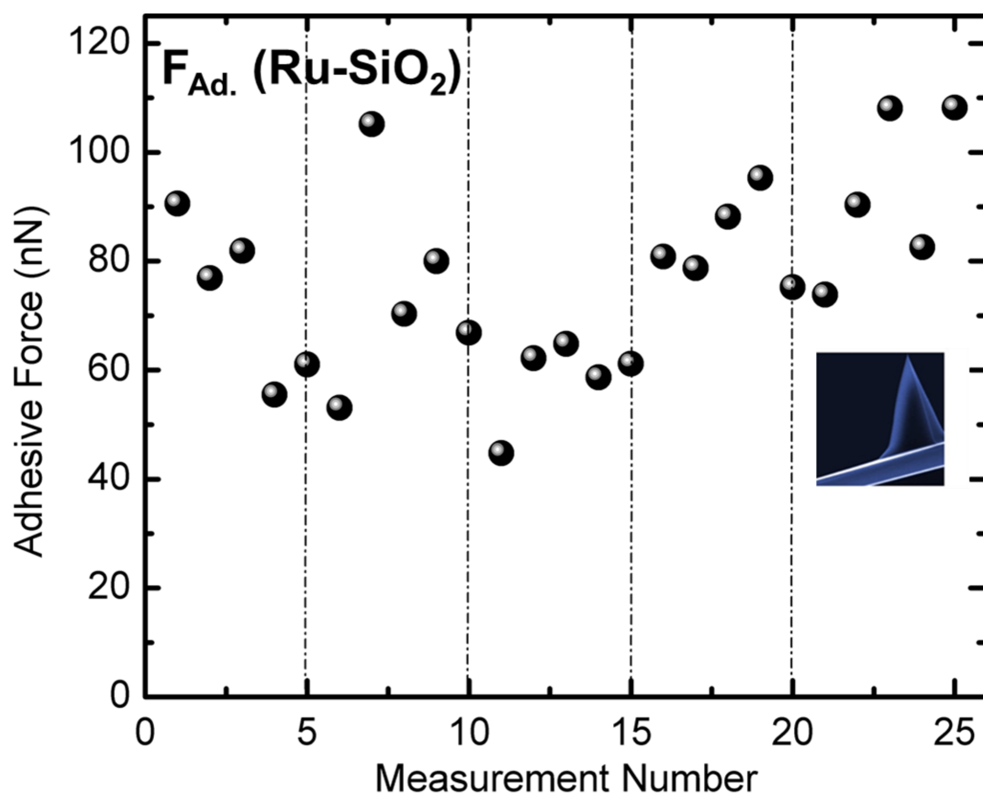

FIG. S2. Measured adhesive force across 50 measurements, for Ru metal films contacted with a bare SiO_2 AFM tip with tip diameter of ~8 nm. Large Standard deviation in measurements suggests that AFM tips with small diameters are not suitable for adhesion measurements.

3. Quantification of Capillary Force

Capillary force due to the presence of water molecules, polymers, and other contaminants can significantly affect measurements of adhesion energy, making a quantitative comparison of adhesion energies of different samples impossible. Jiang et al (Nanoscale, 7, 10760, (2015)) have performed adhesion measurements under different humidity conditions with an AFM tip having a microspherical tip (such as used in this work). Their results show that the measured

adhesive force is not significantly affected when the relative humidity of the measurement environment is less than 25%. The measured adhesive force increases with relative humidity above 25%, by about 14%, and saturates above 40% relative humidity.

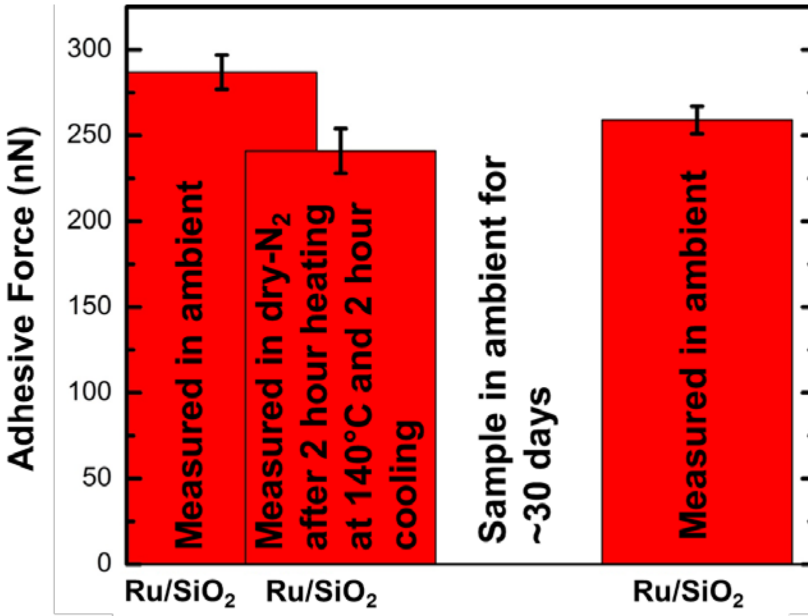

FIG. S3. Adhesive force between Ru-SiO_2 contacts at various processing conditions is presented. The effects of capillary force were overcome by performing the adhesion measurements inside a dry-N_2 chamber, and in-situ annealing of the samples.

The relative humidity in our laboratory usually is between 25% and 35%. To quantify the effect of capillary force, we firstly measured the adhesive force in room ambient, following the experimental procedure described in the paper, performing 10 measurements in each of 10 different areas of the sample. Afterwards we purged the chamber with dry N_2 and heated the sample *in situ* on the AFM stage at 140°C for 2 hours to evaporate any water molecules or low-melting-temperature polymers, and then cooled the sample under dry-N_2 flow for another 2 hours. The AFM tip was kept only 25 μm away from the sample surface during the heat treatment, so that it would be heated as well to remove moisture and other contaminants on its surface. Adhesion measurements were then performed again in each of the 10 different areas of the sample. The measurement results (cf. Fig. S4) consistently show that the dry-N_2 heating treatment results in lower measured adhesive force, by 6% to 13%, indicating that capillary force is not dominant in our measurements.

It is possible that the 140°C heat treatment altered the sample properties, to cause the reduction in measured adhesive force. To rule out this possibility, we stored the sample in room ambient for ~30 days to allow humidity to build up on the surface and then performed the measurement again in room ambient. The increase in measured adhesive force (toward the originally measured value in room ambient) confirms that the heat treatment served only to reduce capillary force.

Table SI1. Ion implantation process parameters for the samples referred to in Fig. S4.

	Implantation conditions			
Wafer ID	**Species**	**Energy [keV]**	**Dose [cm^{-2}]**	**Temp. Control**
Implant-1	O_2	3.0	4.90E+15	Yes
Implant-2	O_2	3.0	4.90E+15	No (uncooled)
Implant-3	O_2	3.0	7.33E+15	Yes
Implant-4	O_2	3.0	7.33E+15	No (uncooled)

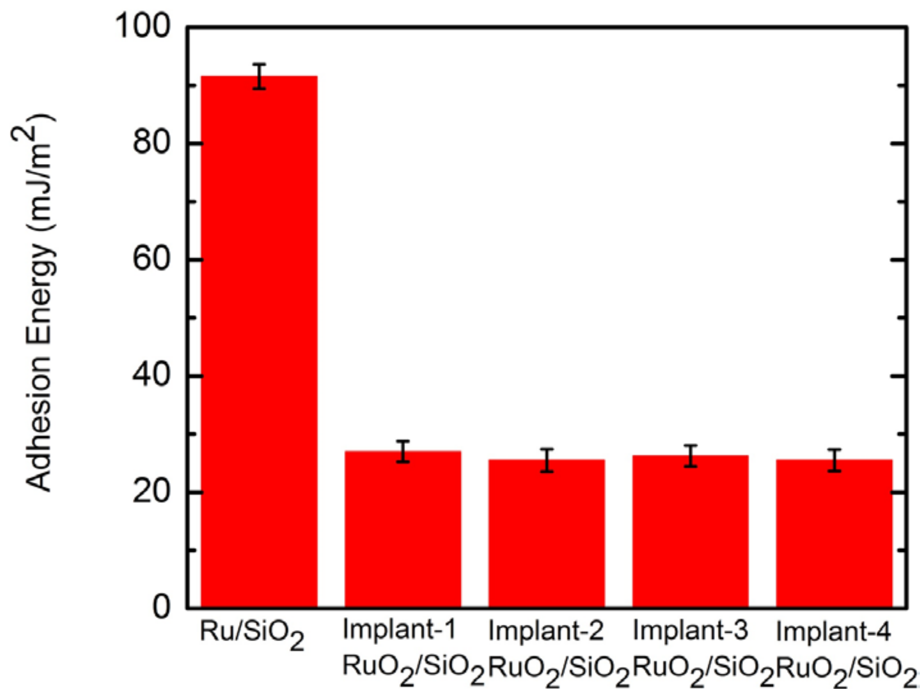

FIG. S4. Adhesive force between Ru-SiO_2 and RuO_2 (prepared by various implantation conditions, but with same annealing recipe)- SiO_2 is presented. The results suggest that three is no significant variations in adhesion energies among the four different RuO_2 films.

4. rms. roughness Sensitivity Test of SiO_2 Spherical Probe

The SiO_2 spherical probe was imaged for its accurate estimate of diameter, but not for its RMS roughness. The probe-tip and roughness were both too small and the curvature of the tip makes it difficult to do normal AFM roughness measurements. However, we have performed a sensitivity test (using equation 1 in the manuscript) of the adhesion energy with respect to the SiO_2 tip roughness, and the results show that the adhesion energy reduction ratio is insensitive to the rms roughness of the tip. The individual adhesion energy value changes with respect to the roughness, as expected.

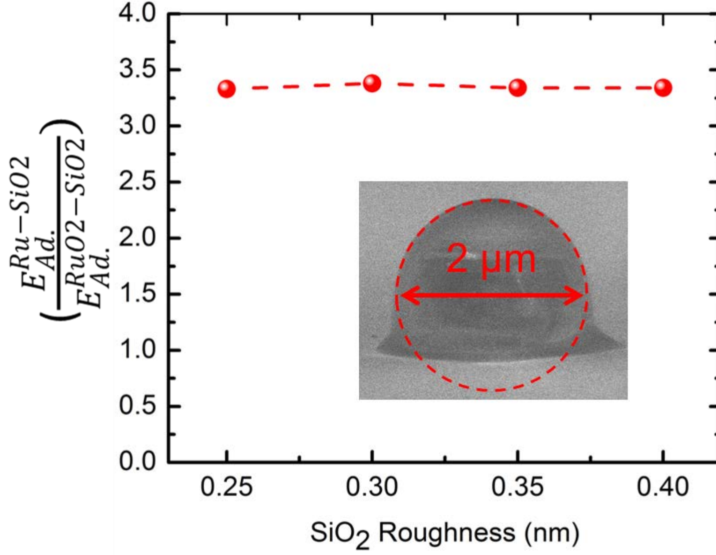

Fig. S5. Adhesive energy reduction ratio between Ru-SiO_2 and RuO_2-SiO_2 contacts are presented as a function of SiO_2 tip rms roughness. SEM image of SiO_2 is presented which show that the tip diameter is exactly 2 μm.

$$W_{Ad.} = \left(\frac{F_{Ad.}}{2\pi R_{tip}}\right)\frac{\left(1+\frac{R_{tip}}{1.48R_{atomic}}\right)^{-1}+\left(1+\frac{1.48R_{atomic}}{z_0}\right)^{-2}}{\left(1+\frac{R_{tip}}{1.48R_{q}}\right)^{-1}+\left(1+\frac{1.48R_{q}}{z_0}\right)^{-2}}, \qquad (1)$$

where $W_{Ad.}$ is the adhesion energy per unit area, $F_{Ad.}$ is the adhesive force determined from AFM measurements, R_{tip} is the radius of the AFM tip, R_{atomic} and R_q are the rms roughness values of the sample surface and the tip, respectively, and z_0 is the equilibrium separation distance between the tip and the sample when they are in contact.

5. Contact Adhesion Force Between SiO_2 and bare-Ru Surface as a Function of Contact Cycle

The contact adhesive force between the SiO_2 and bare-Ru is presented below as a function of the contact cycles as requested. Some differences in the contact adhesive force between the RuO_2/SiO_2 (presented in the manuscript) and the bare-Ru/SiO_2 are observed in these figures. The contact adhesive force in case of the Ru/SiO_2 contacts increases slightly by ~ 6% over the 1000 operating cycles, which is not the case for the RuO_2/SiO_2 interface. The 6% increase in adhesive force for Ru/SiO_2 interface is probably due to wearing of the tips. This result demonstrates that the RuO_2 is a better choice in terms of the contact stability in NEM relay operations.

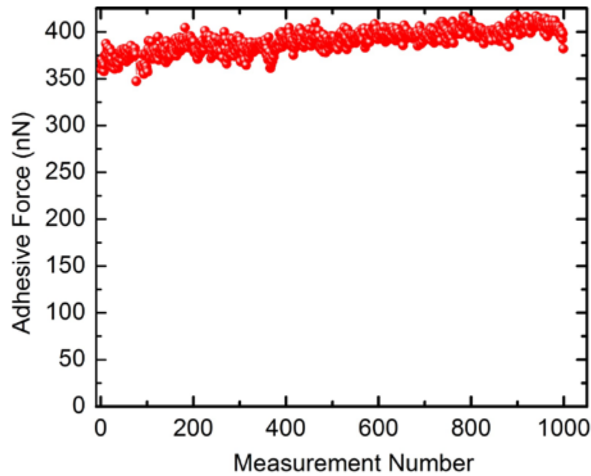

FIG S6. Adhesion cycling test for Ru-SiO2 contacts that shows ~6% increase in adhesive force values over 1000 operating cycles.

6. Effects of AFM characterization frequency on the reliability

We have performed AFM contact stability measurements of adhesive force values between RuO_2-SiO_2 contacts with two different frequencies. The results shown below indicate that there is no significant difference on the reliability between the measurements in 0.25 Hertz and 1 Hertz operating frequencies.

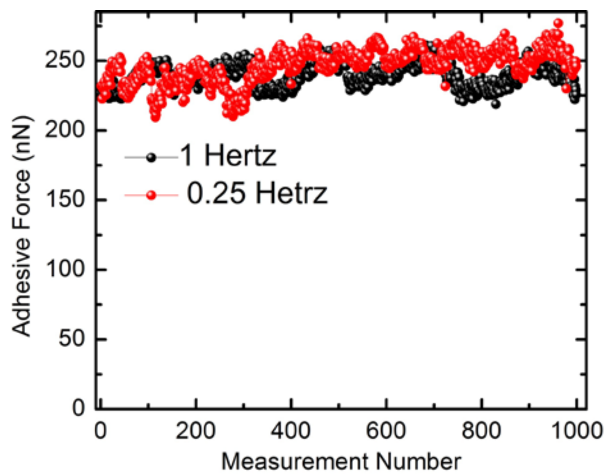

FIG S7: Adhesive force cycling measurement of a RuO_2-SiO_2 contact measured at 0.25 Hertz and 1.00 Hertz operating frequencies.

7. Influence of Electrical Current and Triboelectric Effect on Adhesion in Micro-Relays

The effect of current flow on electrical contacts is an important problem and several books (see P.G. Slade "Electrical contacts: Principle and application", CRC Press Book, 1104pp., 2nd ed, 2013) describe that issue.

During the ON-state, the stiction coefficient may increase with time and with the current due to creep. However, in NEM relays, we can consider that the ON-state is short in time, and the current is low enough, so one does not need to consider the creep effect.

Considering the making and breaking phase of the contact, two behaviors have been observed up to now about stiction coefficient versus operating cycles. At high voltage/current values, a sticking of the contact is observed due to welding of the two contact parts. At lower current, the stiction coefficient decreases with the number of operating cycles, due mostly to the oxidation of the contact. This point is strengthened in the paper by quantifying the loss in adhesion force while the contacts are oxidized.

Triboelectric effect resulting from time dependent charging on the contacts is a potential hazard. The top and bottom contacts are going to be of same materials and the contacts need to be electrically conducting, so the charging will be at least partially released. Secondly, as NEM relays operate in "hot switching" conditions (turning ON/OFF under current), we think that the triboelectric effects are of second order compare to direct electrical effect of the current flow mentioned in the first part of this question. Never the less, these effects are part of our on going investigation and topics for future report.

8. Effects of Relay Packaging conditions on the Adhesion

The adhesion energy of micro-relay contacts could be severely influenced by its packaging conditions such as vacuum, dry-N_2 sealing and humidity. Since humidity will result in unwanted capillary effects on the contacts, the adhesive forces are expected to increase significantly if the relay devices are not packaged. While vacuum packaging is the most desirable; cost and practical limitations may pose limitations. In this respect dry-N_2 packaging might be an effective way to mitigate the capillary effects. Since all of our measurements were performed inside dry-N_2 environment, packaging of relays with dry-N_2 sealing will allow the full benefits of adhesion energy reduction. Further work would be required to understand the details of packaging conditions.